



HAL
open science

Identification and optical features of the $\text{Pb}_4\text{Ln}_2\text{O}_7$ series ($\text{Ln} = \text{La}, \text{Gd}, \text{Sm}, \text{Nd}$); genuine 2D-van der Waals oxides

Marie Colmont, Kévin Lemoine, Pascal Roussel, Houria Kabbour, Jacob Olchowka, Natacha Henry, Hans Hagemann, Olivier Mentré

► To cite this version:

Marie Colmont, Kévin Lemoine, Pascal Roussel, Houria Kabbour, Jacob Olchowka, et al.. Identification and optical features of the $\text{Pb}_4\text{Ln}_2\text{O}_7$ series ($\text{Ln} = \text{La}, \text{Gd}, \text{Sm}, \text{Nd}$); genuine 2D-van der Waals oxides. *Chemical Communications*, 2019, 55 (20), pp.2944-2947. 10.1039/C8CC07707J . hal-03098282

HAL Id: hal-03098282

<https://hal.science/hal-03098282>

Submitted on 22 Nov 2021

HAL is a multi-disciplinary open access archive for the deposit and dissemination of scientific research documents, whether they are published or not. The documents may come from teaching and research institutions in France or abroad, or from public or private research centers.

L'archive ouverte pluridisciplinaire **HAL**, est destinée au dépôt et à la diffusion de documents scientifiques de niveau recherche, publiés ou non, émanant des établissements d'enseignement et de recherche français ou étrangers, des laboratoires publics ou privés.

Identification and optical features of the $\text{Pb}_4\text{Ln}_2\text{O}_7$ series (Ln = La, Gd, Sm, Nd); genuine 2D-van der Waals oxides.

Received 00th January 20xx,
Accepted 00th January 20xx

Marie Colmont,^{*a} Kévin Lemoine,^b Pascal Roussel,^a Houria Kabbour,^a Jacob Olchowka,^{a,c†} Natacha Henry,^a Hans Hagemann,^c and Olivier Mentré^a

DOI: 10.1039/x0xx00000x

www.rsc.org/

We report on the identification and survey of the $\text{Pb}_4\text{Ln}_2\text{O}_7$ series (Ln= La, Gd, Sm and Nd) which turn out to be real Van der Waals 2D oxides. In the neutral layers, strong covalent Pb-O bonds together with external stereoactive Pb^{2+} lonepairs, which play as sensitizers, lead to an ideal matrix for enhanced and tunable luminescence by lanthanide emitters, tested here for Sm^{3+} and Eu^{3+} doping. DFT calculations and preliminary exsolution experiments validate the weak bonding between the layers separated by 3.5 Å and suggest a undirect to direct crossover realized by isolating the layers..

Introduction

Real Van der Waals (VdW) materials offer unprecedented technological properties as each layer acts as the bulk and the interface, revealing highly anisotropic phenomena. In the last decade, several famous phases have dominated the rapid development of 2D materials.¹ Among various singularities, the quantum confinement in single layer MoS_2 TMDC leading to direct/indirect bandgap crossover by increasing the number of stacked layer gives representative example of the emerging physics behind. Particularly, 2D materials are promising, first because of their broad field of applications in optics, electronics, sensors, energy... and secondly because their modularity is an advantage to tune their performances by intercalation of organic/inorganic guests.¹ The further possibility to combine various types of 2D layers in hetero-structures offers extra possibilities for outstanding multi-functional properties, but the diversification of the library of available units is highly demanded. Besides graphene and derivatives,² transition metal dichalcogenides (TMDC), the series of Phosphorene and group

IV-VI compounds (P, SnS, GeS)³ and boron nitrides, only rare examples of real Van der Waals 2D oxides are reported,¹ despite the strong interest of ultrathin oxide layers and the exfoliation and restacking chemistry behind.⁴ Most 2D oxides have layered structures connected by weak covalent or ionic bonds, intercalating elements or oxygen bridges, see Mo/WO_3 , V_2O_5 .^{1,5} In contrast real 2D-VdW compounds are built on neutral blocks with strong intra-covalent bonds. Most often, an active lone pair cation act as a templating low-D agent^{6,7} participating to the stacking interaction such as in the litharge α - PbO (figure 1). In our group, many efforts have been done to create new materials using a predictive approach. It leads to the design of original Bi-based materials using the ability of $6s^2$ lone pair Bi^{3+} cations to form sizeable 2D ribbons/layers stacked into a controlled manner.^{8,9} Besides the fluorite layer archetypes, e.g. $[\text{PbO}]^0$, $[\text{BiO}]^+$ etc..., we have recently evidenced in the compound $\text{PbBi}_4\text{O}_6\text{Cl}_2$ original neutral $[\text{PbBi}_2\text{O}_4]^0$ layers, an inspiring bricks for true 2D-VdW materials. [10] In this paper, we used chemical modifications of the 2D-VdW $\text{Bi}_4(\text{Bi}/\text{La})_2\text{O}_9$ compounds (figure 1),¹¹ to prepare a series of oxygen deficient 2D-VdW analogues $\text{Pb}_4\text{Ln}_2\text{O}_7$ (Ln = La, Gd, Sm, Nd). The confinement of covalent bonds in the blocks together with the presence of Pb^{2+} sensitizers leads to an ideal matrix for enhanced and tuneable luminescence. Preliminary optical properties are given after Sm^{3+} and Eu^{3+} doping of the La compound.

State of the Art

Only few lamellar oxides made of neutral layers are referenced in the literature. Generally speaking, most compounds involve p-element cations with electronic configurations giving rise to an active lone pair (such as Te^{4+} , Se^{4+} , Sb^{3+} ...or Bi^{3+} , Pb^{2+} in our particular case). This lone pair may be seen as the driving agent opening the structure towards low topologies. The richness of the crystal chemistry of bismuth and lead oxides and oxy-salts is governed not only by the labile distorted geometry of the coordination spheres of $\text{Bi}^{3+}/\text{Pb}^{2+}$ ions due to their stereo-active $6s^2$ lone pair,¹² but also by its ability for creating building units of oxo-centered OBi_n polyhedra.¹³

^a Université Lille, CNRS, Centrale Lille, ENSCL, Université Artois, UMR 8181, Unité de Catalyse et Chimie du Solide, Lille, F-59000, France.

^b Université, Université du Maine, CNRS UMR 6283, Institut des Molécules et Matériaux du Mans (IMMM), Avenue Olivier Messiaen, Cedex 9, Le Mans, 72085, France.

^c Dépt. de Chimie Physique, Université de Genève, 30, quai E. Ansermet, Geneva 4, CH-1211, Switzerland.

† Jacob Olchowka actual address is: CNRS, Université Bordeaux, Bordeaux INP, ICMCB UMR 5026, Pessac F-33600, France.

Electronic Supplementary Information (ESI) available: [details of any supplementary information available should be included here]. See DOI: 10.1039/x0xx00000x

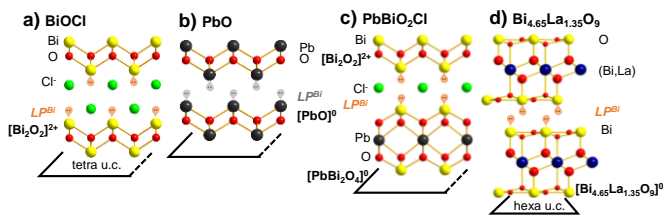


Fig. 1: (a) BiOCl Sillen X_2 -type phase with 2D $[\text{Bi}_2\text{O}_2]^{2+}$ layers, (b) PbO VdW structure with neutral $[\text{PbO}]^0$ layers, (c) PbBiO_2Cl with $[\text{Bi}_2\text{O}_2]^{2+}$ and neutral $[\text{PbBi}_2\text{O}_4]^0$ blocks and (d) $\text{Bi}_{4.65}\text{La}_{1.35}\text{O}_9$ VdW 2D layered structure. Each time, the expected lone pair position (LP) is drawn.

Dealing with 2D topologies, fluorite-type $[\text{BiO}]^+$ or neutral $[\text{PbO}]$ layers are formed by edge-sharing OM_4 tetrahedra. Bi^{3+} based Sillen phases^{14, 15} are relevant 2D-examples built on $[(\text{A},\text{Bi})_2\text{O}_2]$ layers intergrown with single $[\text{X}_1]$, double $[\text{X}_2]$ or triple $[\text{M}'_x\text{X}_3]$ halide layers, where X represents halide atoms.¹⁶ It produces ABiO_2Cl (X_1 -type),¹⁷ BiOCl (X_2 -type, see fig. 1a)¹⁷ and $\text{LiCa}_2\text{Bi}_3\text{O}_4\text{Cl}_6$ (X_3 -type)¹⁸ polytypes with charged modules. Dealing with lead, $[\text{PbO}]$ units are neutral, leading to real VdW-stacking such as in the litharge-PbO (figure 1b)).¹⁹ Combining Pb^{2+} and Bi^{3+} can lead to thicker neutral blocks as observed in more complex intergrowths structures, such as the triple cationic $[\text{PbBi}_2\text{O}_4]^0$ modules found in PbBiO_2Cl (figure 1c)). Beyond PbO, our search in the literature for real 2D-VdW compounds in related phases highlighted the compounds $\text{Bi}_4(\text{Ln}_{2-x}\text{Bi}_x)\text{O}_9$ ($\text{Ln}=\text{La}, \text{Gd}, \text{Nd}$) with more or less extended solid solution domains depending on the Ln size. For large La^{3+} species, it exists in the $0.15 \leq x \leq 0.35$ domain. The structure is monoclinic (P2/c), see Table 1 and rhombohedral above 450°C.¹¹ Here the main cationic lattice is triangular, (fig. 1d) comparatively to the $\text{Bi}^{3+}/\text{Pb}^{2+}$ square lattices of fig.1.a-c. These phases have been the source of inspiration of the current work. The central site is randomly occupied by La^{3+} and Bi^{3+} which involve non-active Bi^{3+} lone pair on this site. Externally at the centre of each Bi-triangle, there is an oxygen leaving OBi_3 units (see fig. 2a). We have tested the possible full substitution of Bi^{3+} for Pb^{2+} in this compound according to the formulation $\text{Bi}_{4-x}\text{Pb}_x\text{Ln}_2\text{O}_9$. Here we rely on significant oxygen non stoichiometry in the external layer. A single phase was obtained for $x=0$, which suggests a full Pb/La ordering. Its unit cell is triclinic, as confirmed latter using single crystal XRD data.

The relationship between the monoclinic and triclinic cells of $\text{Bi}_4(\text{La}_{1.14}\text{Bi}_{0.86})\text{O}_9$ is given by :

$$\begin{pmatrix} a_{\text{mono}} \\ b_{\text{mono}} \\ c_{\text{mono}} \end{pmatrix} = \begin{pmatrix} 0 & 0 & 1 \\ \frac{1}{2} & -\frac{1}{2} & 0 \\ \frac{1}{2} & \frac{1}{2} & 0 \end{pmatrix} \begin{pmatrix} a_{\text{tric}} \\ b_{\text{tric}} \\ c_{\text{tric}} \end{pmatrix}$$

For other Pb/Ln case ($\text{Ln} = \text{Gd}, \text{Sm}, \text{Nd}$), the XRD patterns reveal a main monoclinic symmetry similar to the parent La/Bi phase, with a set of extra-peaks not well understood yet. Their full crystal structure will be published elsewhere. The refined lattice parameters are listed in Table 1 together with the antagonist cationic radii. In this paper we will focus on the Pb/La and its luminescent properties after 10% Sm^{3+} and Eu^{3+} substitution for La^{3+} .

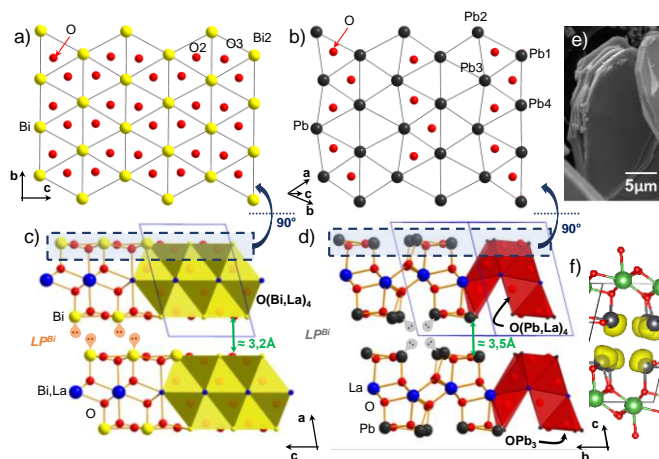


Fig. 2: Bismuth/Lead oxygen environments in external part of neutral layers in (a) $\text{Bi}_{4.65}\text{La}_{1.35}\text{O}_9$ and (b) $\text{Pb}_4\text{La}_2\text{O}_7$; crystal structure of (c) $\text{Bi}_{4.65}\text{La}_{1.35}\text{O}_9$ and (d) $\text{Pb}_4\text{La}_2\text{O}_7$.

An SEM image is added in insert to enhance the layered behaviour at the micro scale, (e) SEM image with the layers and (f) ELF representation of lone pair electrons.

Table 1: Unit cell parameters of all $\text{Pb}_4\text{Ln}_2\text{O}_7$

$\text{Ln}^{3+}/\text{M}^{2+}$ ($r_{\text{Ln}^{3+}}/r_{\text{M}^{2+}}$)	a(Å)	$\alpha(^{\circ})$	b(Å)	$\beta(^{\circ})$	c(Å)	$\gamma(^{\circ})$	v(Å ³)
$\text{La}^{3+}/\text{Pb}^{2+}$ (1.03/1.19)	7.7054(10)	72.574(10)	7.7262(10)	84.285(10)	10.1822(10)	61.737(10)	508.77(12)
$\text{Gd}^{3+}/\text{Pb}^{2+}$ (0.938/1.19)	6.4148(3)	90	3.8194(2)	91.55(1)	9.6606(4)	90	236.59(2)
$\text{Nd}^{3+}/\text{Pb}^{2+}$ (1.29/1.19)	6.3243(7)	90	3.8434(4)	91.00(10)	9.6785(10)	90	235.22(6)
$\text{Sm}^{3+}/\text{Pb}^{2+}$ (1.22/1.19)	6.4558(5)	90	3.8506(2)	91.65(6)	9.6708(7)	90	240.30(4)
$\text{La}^{3+}/\text{Bi}^{3+}$ (1.03/1.03)	9.4956(3)	90	3.9742(1)	104.700(2)	7.0425(2)	90	257.07

The crystal structure of the new $\text{Pb}_4\text{La}_2\text{O}_7$ was refined from single-XRD data, and is compared to the Bi/La one on Figure 2. It is built on 2D-neutral thick layers, with weak interactions between them, as easily observed on SEM images showing a self-exfoliated microstructure (figure 2d). In terms of oxo-centred units, the layer is built on the association of OPb_3La , OPbLa_3 and OPb_3^0 oxo-centred units sharing edges. Contrarily to the reported Bi/La random distribution in the central site, here a full La/Pb ordering exists, La^{3+} taking place at the centre of the blocks whereas Pb^{2+} stands at their edges so that the Pb^{2+} lone pairs (LP) are pointing outwards (figure 2d). All Pb atoms form OPb_3 tetrahedra tilted such that the LP point not perpendicular to the layers contrary to the Bi case where the Bi-LP have a larger radial expansion inside the interleaves. The main difference arises from external layer of triangular Pb^{2+} due to the ordering of oxygen vacancies shown on Fig. 2b. The Pb-Pb distances in the layer are around 3.6 Å whereas there are of 4.6 Å between two successive layers. Such ordering of vacancies in the Pb/La phase are responsible for the volume doubling, not detected by XRD on polycrystalline samples of the other Pb/Ln compounds. However the extra peaks mentioned for Gd/Pb, Nd/Pb and Sm/Pb phases plausibly denote another kind of oxygen/vacancy ordering within the main monoclinic framework. The symmetry lowering to triclinic and splitted XRD peaks was only observed for the La/Pb compound and is plausibly related to a critical Ln^{3+} radius compared to the one of the external Pb^{2+} or Bi^{3+} cation, see Table 1. The external

Localization of the LP was verified using the Verbaere method implemented in the Hybride program, see Table S2.^{22,23}

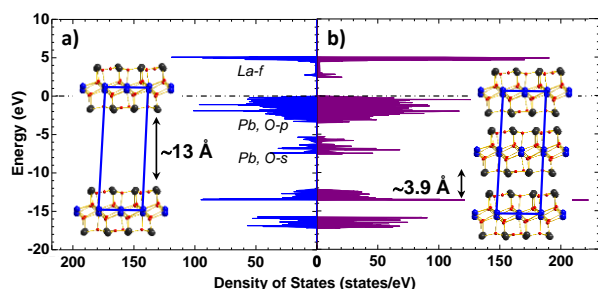


Fig. 3: Total density of states (DOS in state/eV per cell) calculated a) for one isolated single layer and b) for the complete unit cell.

According to the La^{3+} vs Pb^{2+} ionic radii playing for a triclinic symmetry, and Pb^{2+} lone pairs, the average $\langle \text{Pb-O} \rangle$ and $\langle \text{La-O} \rangle$ distances are inhomogeneous, 2.20 to 2.48 Å and 2.34 to 2.56 Å respectively. The local charges were calculated using the Henry's model implemented in Winpacha, using non empirical scales of atomic electronegativity and hardness.^{24, 25} It gives results of the Table S2 with in average *ca.* -0.8 and -0.5 on core and external oxygen respectively and *ca.* +0.1 and +2 on Pb and La, respectively as expected for covalent Pb-O bonds versus ionic-covalent La-O ones. Finally, the stability of the structure is achieved by weak VdW interactions, taking into account next layers distant of about 3.9 Å. Here local charges and LP electrons interact by dipolar couplings.

The reactivity is strongly related to the partial charges at the surface of the layers. Contrary to the Bi-phase the Pb one rapidly degrades under air through H_2O and CO_2 uptake giving $\text{Pb}_3(\text{CO}_3)_2(\text{H}_2\text{O})_2$, LaCO_3OH , $\text{La}_{1.73}\text{Pb}_{2.27}\text{O}_{6.20}$, Pb_2OCO_3 and several lead oxides (more details in SI). This phenomenon is fully reversible after heating at 900°C during several hours.

2D-VdW phases

The Weakly interacting blocks into a 2D electronic topology was checked by band structure calculation performed using the DFT code VASP, see S7. The Figure 3 shows the total density of states calculated both for the entire crystal structure and exaggeratedly isolated 2D layer after removal of every other layer. The calculated indirect (see band structure in S7) bandgap is 2.32 eV, lower than the experimental 3.12 eV value, a common underestimation dealing with GGA calculations. The contribution to the valence and conduction bands are detailed in S7, but occupied and unoccupied levels show well separated features with specific contributions, signing weak electronic interactions between the $[\text{Pb}_4\text{O}_3]$ and $[\text{La}_2\text{O}_4]$ units, in agreement with the local charges discussed above. Below the Fermi level, Pb *p* states and O *p* states overlap with a small contribution of the Pb *s* states just below the Fermi level, while the bottom of the conduction band is dominated by La *f* (around 4.8 eV) states with a small contribution of Pb *p* states (around 2.7 eV). As expected, from a qualitative point of view, the contribution of one isolated layer is almost identical to that of the 3D structure as reported for α - PbO .¹⁹ However in the latest, the main effect of the stacking is the broadening of the highest occupied bands, indicating a certain degree of bonding between lead atoms of two next layers. This effect

is minor in the title compound, signing very weak interlayer bonds, related to their lowest surficial charges, and the weakest lone pair expansion in the interleaves, see figure 2d. Preliminary measurements suggest an indirect to direct bandgap crossover going to isolated layers (see S7). The main picture based on the weak Van der Waals interactions between the blocks is also corroborated by the similar partial charges calculated for single and stacked layers (Table S4). Finally, the electron localization function (ELF), allowed the visualization of the nodal structure of the molecular orbital, including lone pair electrons.²² Figure 2f represents 3D isosurfaces at ELF value 0.9. The LP are inclined outwards the layers as described above.

Preliminary exsolution results

In order to show the real Van der Waals behavior, a mechanical exfoliation was performed using ball milling (ZrO_2 bowl and balls). After few minutes (5 to 10) a broadening of peaks on XRD occurs, prior to amorphization of the sample after 30 min (see SI 8). The XRD pattern shows a broad maximum around $d=3.2\text{Å}$ (i.e. d_{220}) which suggests exfoliation of the layer with conservation of the in-plane organization. Exfoliation was also performed after long-time stirring in specific solvent and will be published elsewhere. So far, the best result was obtained in butanol. A TEM study proved the presence of very thin sheets with weak opacity. Additional DLS and Potential Zeta study highlight neutral nano flakes and a size distribution centered around 225nm (see SI 8).

Optical properties

Lanthanide-based materials play a crucial role in solid state lighting, since they are often used as activator in many commercial phosphors for LED application such as the yellow-emitting $\text{Y}_3\text{Al}_5\text{O}_{12}:\text{Ce}^{3+}$ or the red-emitting $\text{Y}_2\text{O}_3:\text{Eu}^{3+}$.^{23,24} Indeed, finding new phosphors especially 2D matrix with lone pair (Pb^{2+}) emitters is relevant for plenty of reasons. The 2D character lead to i) shortest Pb-O distances (intra layer) and ii) strongest lone pair activity outward. If the former play for a redshift of the excitation energy due to both the nephelauxetic effect, the LP stereoactivity tune the stoke shift shifting the excited-state potential relative to the ground state, during the $6s^2 \rightarrow 6p$ transition, see ref.^{16,25} iii) In addition, one benefits of the large absorption section and broad spectra of ns^2 cations able to charge transfer via oxygen ligands. $\text{Pb}_4\text{La}_2\text{O}_7$ contains Pb^{2+} ions that can act as activators,¹⁰ but no room temperature emission can be detected, most probably due to a concentration quenching. On the opposite, doping with Eu^{3+} or Sm^{3+} ions leads to bright RT reddish-orange emission (respectively CIE coordinates $x=0.5412$, $y=0.4102$ and $x=0.5614$, $y=0.3913$, see figure 4). Figure 4)a,b shows the RT excitation and emission spectra of $\text{Pb}_4\text{La}_2\text{O}_7:\text{Ln}^{3+}$ ($\text{Ln}=\text{Eu}, \text{Sm}$). Here, it is reasonable to suppose that Eu^{3+} and Sm^{3+} cations take place in one or both of Lanthanum sites, due to the similarity of ionic radius and also especially due to the same oxidation state.

The excitation spectra of both Sm^{3+} ($\lambda_{\text{em}} = 651 \text{ nm}$) and Eu^{3+} ($\lambda_{\text{em}} = 612 \text{ nm}$) 10% doped $\text{Pb}_4\text{La}_2\text{O}_7$ (on the La site) show a broad asymmetrical band peaking with sharp maxima around 400 nm. This is strongly redshifted compared to the common excitation energies in LP Bi^{3+} or Pb^{2+} phosphors (*ca.* 250-350 nm) phosphors, and maybe assigned to the strong Pb-O interactions in the PbO_3 groups due to

the 2D character. The discrete peaks at lower energy are assigned to 4f-4f lanthanide transitions, e.g. sharp Sm^{3+} : ${}^7\text{F}_0 \rightarrow {}^5\text{D}_2$ at 466 nm, see Fig. 4a. The broad excitation bands match well the reflectance spectrum shown figure 4c and correspond to the host-lattice absorption for which a contribution of a $(\text{Pb})\text{-O}(2\text{p}) \rightarrow \text{Ln}(4\text{f})$ charge transfer is active²⁵. From the PDOS calculations, it was shown that the 6s and 6p states of Pb are respectively localized at the top of the VB and the bottom of the CB, leading to host absorption mainly driven by the Pb^{2+} : $6\text{s}^2 \rightarrow 6\text{p}$ transitions and so it can be assumed that Pb^{2+} play the role of sensitizer. As for the undoped compound, the typical Pb^{2+} emission broad band is not observed (quenching) but only very intense lanthanide transitions are observed, scaled by the intense excitation/absorption band.

After Sm^{3+} doping, the reddish-orange light emission consists of the typical four groups of sharp peaks with maximum at 566/572, 603/611, 651/662 and 717nm assigned to Sm^{3+} transitions from the excited level ${}^4\text{G}_{5/2}$ to the ground levels ${}^6\text{H}_{5/2}$, ${}^6\text{H}_{7/2}$, ${}^6\text{H}_{9/2}$, ${}^6\text{H}_{11/2}$ respectively (intra-4f-shell transitions). The monoexponential decay time ($\lambda_{\text{ex}}=397\text{nm}$ and $\lambda_{\text{em}}=651\text{nm}$) was fitted to 0.99 ms, as expected for forbidden f-f transitions.²⁶

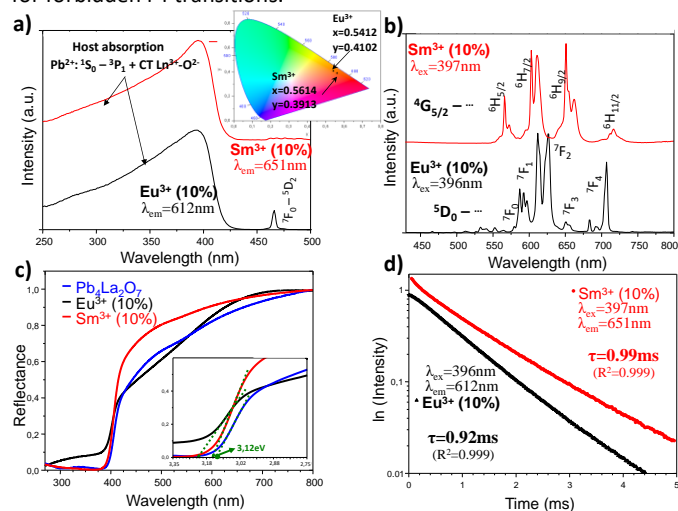


Fig. 4: (a) excitation and (b) emission spectra, (c) UV spectra and (d) decay time ($\lambda_{\text{ex}}=396\text{nm}$ and $\lambda_{\text{em}}=612\text{nm}$) of $\text{Pb}_4\text{La}_2\text{O}_7$: Ln^{3+} ($\text{Ln}=\text{Eu}$ and Sm). In c), UV spectrum of the non-doped sample is added for comparison. CIE 1931 colour space diagram with colour coordinates of $\text{Pb}_4\text{La}_2\text{O}_7$:10% Sm^{3+} and Eu^{3+} is added on insert.

The Eu^{3+} doped compound shows the most intense ${}^5\text{D}_0 \rightarrow {}^7\text{F}_2$ so-called “hypersensitive transition”, responsible for the Eu^{3+} reddish emission of this material. It is represented by a doublet (max at 612 and 626 nm) with a shoulder-like splitting for each. Other low intense peaks are assigned on the figure 8b. Among them, both the weakness of the ${}^5\text{D}_0 \rightarrow {}^7\text{F}_0$ transition at 580 nm and the ${}^5\text{D}_0 \rightarrow {}^7\text{F}_1$ triplet (magnetic dipole transition) at 587, 593 and 597nm are in agreement with the low site-symmetry of the Eu^{3+} site in the triclinic symmetry.²⁷ The decay time of the most intense transition was measured at RT ($\lambda_{\text{ex}}=396\text{nm}$ and $\lambda_{\text{em}}=612\text{nm}$, see figure 4d)) and can be fitted with a monoexponential behavior to 0.92 ms very similar to the Sm^{3+} case.

We identified the new $\text{Pb}_4\text{Ln}_2\text{O}_7$ series ($\text{Ln}=\text{La}$, Gd , Sm and Nd), a rare example of real Van der Waals 2D oxides. They arise from the full substitution of Pb^{2+} for Bi^{3+} in $\text{Bi}_4\text{Ln}_2\text{O}_9$ giving an oxygen labile playground for anionic transport currently under investigation. The weakly interacting layers were confirmed by DFT and partial charges calculations using stacked or individual layers. The resulting 2D character is particularly pronounced here, playing for easy

degradation in air as experimentally observed. This 2D material is particularly interesting because of its large absorption section and broad spectra in the UV domain with a maximum around 400nm driven by Pb-O interaction at the Fermi level. That gives the possibility to be a host-sensitizer for several trivalent lanthanides (Eu^{3+} , Sm^{3+} ...) that usually exhibit low absorption cross sections inducing low emission intensity. Its easy exfoliation will be exploited for preparation of optically active ultrathin objects.

Conflicts of interest. There are no conflicts to declare.

Notes and references

- Supplementary Information containing experimental information, crystal data and structural and experimental parameters.
- K. S. Novoselov, A. Mishchenko, A. Carvalho, and A. H. Castro Neto, *Science*, 2016, **353**, aac9439.
- A. Narita, X.-Y. Wang, X. Feng, and K. Müllen, *Chem Soc Rev*, 2015, **44**, 6616–6643.
- R. Irshad, K. Tahir, B. Li, Z. Sher, J. Ali, and S. Nazir, *J. Ind. Eng. Chem.*, 2018, **64**, 60–69.
- F. P. Netzer and A. Fortunelli, Eds., *Oxide Materials at the Two-Dimensional Limit*, vol. 234. Cham: Springer International Publishing, 2016.
- S. Sucharitakul, G. Ye, W.R.L. Lambrecht, C. Bhandari, A. Gross, R. He, H. Poelman, X.P.A. Gao, *ACS Appl. Mater. Interfaces*, 2017, **9**, 23949–23956.
- R. Becker, M. Johnsson, R. K. Kremer, H.-H. Klaus, and P. Lemmens, *J. Am. Chem. Soc.*, 2006, **128**, 15469–15475.
- M. Johnsson, K. W. Törnroos, P. Lemmens, and P. Millet, *Chem. Mater.*, 2003, **15**, 68–73.
- M. Huvé, M. Colmont, J. Lejay, P. Aschehoug, and O. Menétré, *Chem. Mater.*, 2009, **21**, 4019–4029.
- M. Colmont, M. Huvé, F. Abraham, and O. Menétré, *J. Solid State Chem.*, 2004, **177**, 4149–4162.
- A. Aliev, J. Olchowka, M. Colmont, E. Capoen, C. Wickleder, and O. Menétré, *Inorg. Chem.*, 2013, **52**, 8427–8435.
- M. Drache, P. Roussel, and J.-P. Wignacourt, *Chem. Rev.*, 2007, **107**, 80–96.
- N. Corneil, N. Tancret, F. Abraham, and O. Menétré, *Inorg. Chem.*, 2006, **45**, 4886–4888.
- S. V. Krivovichev, O. Menétré, O. I. Siidra, M. Colmont, and S. K. Filatov, *Chem. Rev.*, 2013, **113**, 6459–6535.
- B. Aurivillius, J. Albertson, G. Svensson, L. Ebersson, P. Krogsgaard, K. Maartmann, S. Wold, *Acta Chem. Scand.*, 1990, **44**, 111–122.
- M. Mercurio, M. E. Farissi, J. C. Champarnaud-Mesjard, B. Frit, P. Conflant, and G. Roult, *J. Solid State Chem.*, 1989, **80**, 133–143.
- J. Olchowka, H. Kabbour, M. Colmont, M. Adlung, C. Wickleder, and O. Menétré, *Inorg. Chem.*, 2016, **55**, 7582–7592.
- D. Charkin, P. Berdonosov, V. Dolgikh, and P. Lightfoot, *J. Solid State Chem.*, 2003, **175**, 316–321.
- S. Lopatin S, *Ž. Neorg. Him.*, 1987, **32**, 1694–1697.
- B. Dickens, *J. Inorg. Nucl. Chem.*, 1965, **27**, 1503–1507.
- A. Verbaere, R. Marchand, and M. Tournoux, *J. Solid State Chem.*, 1978, **23**, 383–390.
- E. Morin, G. Wallez, S. Jaulmes, J. C. Couturier, and M. Quarton, *J. Solid State Chem.*, 1998, **137**, 283–288.
- B. Silvi and A. Savin, *Nature*, 1994, **371**, 683–686.
- P. Gorrotxategi, M. Consonni, and A. Gasse, *J. Solid State Light.*, 2015, **2**, 1.
- J. Lian, H. Qin, P. Liang, and F. Liu, *Solid State Sci.*, 2015, **48**, 147–154.
- J. Olchowka, M. Colmont, H. Kabbour, O. Menétré, *Chem. - Eur. J.*, 2017, **23**, 15694–15703.
- G. H. Dieke, H. M. Crosswhite, and H. Crosswhite, “Spectra and energy levels of rare earth ions in crystals,” Interscience Publishers., New York, 1968.
- K. Binnemans, *Coord. Chem. Rev.*, 2015, **295**, 1–45.